

The disc-jet coupling in the neutron star X-ray binary Aquila X-1

V. Tudose,^{1,2,3,*}† R.P. Fender,^{4,1} M. Linares,¹ D. Maitra¹ and M. van der Klis¹

¹*Astronomical Institute ‘Anton Pannekoek’, University of Amsterdam, Kruislaan 403, 1098 SJ Amsterdam, the Netherlands*

²*Astronomical Institute of the Romanian Academy, Cutitul de Argint 5, RO-040557 Bucharest, Romania*

³*Research Center for Atomic Physics and Astrophysics, Atomistilor 405, RO-077125 Bucharest, Romania*

⁴*School of Physics and Astronomy, University of Southampton, Highfield, Southampton SO17 1BJ*

Accepted 2009 August 24. Received 2009 August 24; in original form 2008 November 26

ABSTRACT

We study the accretion/ejection processes (i.e. disc/jet coupling) in the neutron star X-ray binary Aquila X-1 via a multi-wavelength approach. We use in the radio band the publicly available Very Large Array archive containing observations of the object between 1986–2005, in the X-ray band the archival Rossi X-ray Timing Explorer data (Proportional Counter Array and High Energy X-ray Timing Experiment) between 1997–2008, and in optical (R band) observations with the Small and Moderate Aperture Research Telescope System recorded between 1998–2007. In the combined data set we find three outbursts for which quasi-simultaneous radio, optical (R band) and X-ray data exist and focus on them to some extent. We provide evidence that the disc/jet coupling in Aquila X-1 is similar to what has been observed in black hole X-ray binaries, at least from the point of view of the behaviour in the hardness-intensity diagrams (the hysteresis effect included), when the phenomenology of the jet is taken into account. Although based on a very small number of observations, a radio/X-ray correlation seems to exist for this system, with a slope of $\alpha=0.40 \pm 0.07$ ($F_{\text{radio}} \propto F_X^\alpha$), which is different than the slope of $\alpha=1.40 \pm 0.25$ found for another atoll source, 4U 1728-34, but interestingly enough is relatively close to the values obtained for several black hole X-ray binaries. No significant correlation is found between the radio and optical (R band) emissions. We also report a significant drop in the radio flux from Aql X-1 above an X-ray flux of $\sim 5 \times 10^{-9}$ erg cm⁻² s⁻¹. This behaviour, also reported in the neutron star X-ray binary 4U 1728-34, may be analogous to the suppression of radio emission in black hole X-ray binaries in bright, soft X-ray states. It suggests that from this point of view neutron star X-ray binaries can mimic the behaviour of black hole X-ray binaries in suppressing the jet in soft/disc-dominated X-ray states.

Key words: accretion, accretion discs – stars: individual: Aquila X-1 – ISM: jets and outflows – radiation mechanisms: non-thermal – X-rays: stars.

1 INTRODUCTION

The low-mass X-ray binary (LMXRB) Aquila X-1 (Aql X-1) is a recurrent soft X-ray transient which shows quasi-periodic outbursts about once a year (Priedhorsky & Terrell 1984; Kitamoto et al. 1993; Šimon 2002). The compact object in the system is a neutron star as implied by the detection of type I X-ray bursts (e.g. Koyama et al. 1981; Czerny et al. 1987; Yu et al. 1999). The companion is a main

sequence star likely of the spectral type K7 (Chevalier et al. 1999). The X-ray timing and spectral properties of Aql X-1 place it in the class of atoll sources (Reig et al. 2000) and recent observations of coherent pulsations in the persistent X-ray emission (Casella et al. 2008) makes it the ninth accretion-powered millisecond X-ray pulsar (AMP) known to date. The atolls show two main X-ray states (Hasinger & van der Klis 1989; van der Klis 1989), identifiable in the colour-colour diagrams: a softer, “banana state” (BS), and a harder, “island state” (IS). In order to accommodate later observations of harder X-ray spectra a new state was defined (e.g. Prins & van der Klis 1997): the “extreme island state” (EIS). From the point of view of the

* E-mail: tudose@astron.nl (VT)

† Present address: Netherlands Institute for Radio Astronomy, Oude Hoogeveensedijk 4, 7991 PD Dwingeloo, the Netherlands

X-ray spectral and timing properties, atoll sources (especially in the EIS) share many properties with the black hole XRBs (BHXRBs) in the low-hard state (e.g. van der Klis 1994; Olive et al. 1998; Berger & van der Klis 1998).

Aql X-1 also exhibits X-ray burst oscillations (e.g. Zhang et al. 1998) and kHz quasi-periodic oscillations (QPOs), both lower kHz QPO (e.g. Cui et al. 1998; Méndez, van der Klis & Ford 2001; Reig, van Straaten & van der Klis 2004), and upper kHz QPO (a single detection, Barret, Boutelier & Miller 2008).

The optical counterpart has in quiescence a V band magnitude of 21.60 and is only $0''.48$ away from a contaminating star of V band magnitude 19.42 (Chevalier et al. 1999) thus complicating the optical studies.

Besides the orbital period close to 19 h (Chevalier & Ilovaisky 1991, 1998; Shahbaz et al. 1998; Welsh, Robinson & Young 2000), little is known about the other parameters of the system. The inclination of the orbit is poorly constrained, with values ranging between 36° and 70° (Shahbaz, Casares & Charles 1997; Garcia et al. 1999; Welsh, Robinson & Young 2000). The distance to Aql X-1 is not well known, but different estimates place it in the range 4–6.5 kpc (Chevalier et al. 1999; Rutledge et al. 2001; Jonker & Nelemans 2004).

Reports of radio observations of Aql X-1 are extremely scarce in the literature: Hjellming, Han & Roussel-Dupre (1990); Rupen, Mioduszewski & Dhawan (2004, 2005). To date, only five radio detections have been documented, all obtained by the VLA during outbursts: four at 8.4 GHz (two in 1990 August and two in 2004 May), and one at 4.9 GHz (in 2005 April). This is not surprising since the atoll sources are quite difficult to observe given their sub-mJy flux density levels at cm wavelengths even during outbursts (Fender & Kuulkers 2001). Basically, although they represent the bulk of the XRBs population (Fender 2006), only a handful of atoll sources have been detected in radio (e.g. Hjellming & Han 1995; Martí et al. 1998; Migliari et al. 2003, 2004; Moore et al. 2000). In the case of the atoll source 4U 1728-34 a correlation was found between the radio and X-ray fluxes in the hard state (Migliari et al. 2003; Migliari & Fender 2006), resembling the relation established for BHXRBs in the low-hard state (Corbel et al. 2003; Gallo, Fender & Pooley 2003; Gallo et al. 2006; Corbel, Körding & Kaaret 2008, but see also Xue & Cui 2007), but with a steeper gradient.

2 OBSERVATIONS

2.1 Radio

We have analyzed all the public Very Large Array (VLA) radio data between 1986 February and 2005 December containing observations of Aql X-1 (close to 100 epochs). The majority of the observations were carried out at multiple frequencies, particularly at 4.9 and 8.4 GHz. Other frequencies, namely 1.5 and 15.0 GHz, were observed much less frequently. The bandwidth used was 100 MHz. All the runs were performed after reports of increased activity from Aql X-1 mainly at optical and X-ray wavelengths, and thus generally trace the outburst history of the object. Given the

target of opportunity nature of the observations, the array configurations were varying between runs, and the effective observing time ranged roughly between 5 and 60 min, with the median around 10–20 min. Primary calibrators were either 3C286 or 3C48. As secondary calibrators we used, upon availability, J1950+081 or J1925+211 for the vast majority of the epochs, J1922+155, J1939-100, J2007+404, J1851+005, or J1820-254. The data were calibrated in AIPS04 using standard procedures as highlighted in Diamond (1995). The imaging was done in DIFMAP 2.4e (Shepherd 1997) by progressively cleaning the residual map using the CLEAN algorithm of Högbom (1974). The uv -plane fitting was carried out with elliptical Gaussians within the same software.

We detected Aql X-1 at more than 3σ levels on 7 epochs at 8.4 GHz (Table 1) and 4 epochs at 4.9 GHz (Table 2). In two occasions the detections were quasi-simultaneous at both frequencies. At least in the cases of some outbursts it is likely that the lack of detection in the radio band is partly due to the very short integration times which generated relatively high noise levels. In Tables 1 and 2 we also include the upper limits (3σ) of the flux densities for the observations pertaining to outbursts for which there are radio detections.

When detected, the object was unresolved. All the flux densities reported here are determined via uv -plane fitting and the corresponding errors are estimated based on the rms noise of the images and the differences between flux densities measured in the uv -plane using different initial conditions. Two contaminating sources are present in the field of view, ~ 40 and ~ 290 arcsec away from the position of Aql X-1, and affect the quality of the images in compact configurations at lower frequencies (i.e. 4.9 GHz). However, this should not significantly influence the flux measurements. Our values are in agreement, within the errors, with those reported by Hjellming et al. (1990) and Rupen et al. (2004, 2005). The only exception is the data at 4.9 GHz from 2005 April (MJD 53465.54) when we clearly detect the target while in the previous work only a marginal detection is noted. This inconsistency comes probably from a misidentification of the source on this particular epoch. Generally speaking, the radio flux density levels of Aql X-1 are relatively low. At times, noise features are present in the radio maps and can be misidentified as the target. This could have happened on this instance we mention.

2.2 X-ray

We used archival Rossi X-ray Timing Explorer (RXTE) Proportional Counter Array (PCA) and High Energy X-ray Timing Experiment (HEXTE) data of Aql X-1 available in NASA's High Energy Astrophysics Science Archive Research Center (HEASARC).

We filtered out data taken when the spacecraft was pointing away from the source (offset > 0.02 degrees), too close to the Earth (elevation < 10 degrees) or during and up to 15 minutes after the South Atlantic Anomaly passages. All RXTE products were extracted using the standard HEASOFT tools (version 6.5).

In the case of the PCA, the count rates were extracted using the Standard 2 data of all active PCUs (with 16 s time resolution) and averaged over each observation. Following previous work (e.g. Reig et al. 2004) we used the following

Table 1. The VLA 8.4 GHz radio detections and a selection of upper limits (3σ) together with the corresponding quasi-simultaneous observations in optical (R band) and X-ray (PCA/RXTE and HEXTE/RXTE) bands.

Date	MJD radio [day]	Flux density radio [μ Jy]	MJD optical [day]	Flux density optical [μ Jy]	MJD PCA [day]	Flux PCA [10^{-9} erg cm $^{-2}$ s $^{-1}$]	MJD HEXTE [day]	Count rate HEXTE [c s $^{-1}$]	X-ray state
1990 August	48111.23	415 \pm 38	-	-	-	-	-	-	-
1990 August	48129.23	150 \pm 21	-	-	-	-	-	-	-
2002 March	52334.62	< 69	52334.39	372 \pm 12	52335.04	5.57 \pm 0.56	52332.92	1.1 \pm 0.3	BS
2002 March	52355.67	179 \pm 26	52354.87	302 \pm 10	52355.84	1.40 \pm 0.20	52356.69	2.3 \pm 0.4	IS
2002 April	52379.60	< 68	-	-	-	-	-	-	-
2002 May	52399.58	< 57	52400.82	16 \pm 2	-	-	-	-	-
2002 May	52413.52	< 63	52414.29	1 \pm 2	-	-	-	-	-
2004 March	53073.71	< 183	-	-	53074.90	1.26 \pm 0.11	53074.91	11.3 \pm 0.3	EIS
2004 March	53077.48	< 147	-	-	53078.84	1.06 \pm 0.11	53078.84	8.7 \pm 0.3	EIS
2004 March	53085.56	< 174	-	-	53085.93	1.06 \pm 0.11	53085.93	9.2 \pm 0.3	EIS
2004 March	53091.56	< 150	53092.38	297 \pm 10	53088.90	0.84 \pm 0.21	-	-	EIS
2004 May	53144.50	179 \pm 22	53144.36	610 \pm 19	53144.63	1.44 \pm 0.14	53143.65	16.1 \pm 0.7	EIS
2004 May	53151.42	216 \pm 19	53151.35	793 \pm 24	53151.71	1.97 \pm 0.13	53151.71	17.1 \pm 0.4	EIS
2004 June	53162.37	205 \pm 19	53162.38	540 \pm 17	53162.67	2.41 \pm 0.20	53162.67	17.3 \pm 0.4	EIS
2004 June	53170.35	274 \pm 22	53169.40	440 \pm 14	53170.40	3.89 \pm 0.51	53172.37	0.6 \pm 0.5	BS
2004 June	53176.29	< 114	53177.15	121 \pm 5	53176.92	0.40 \pm 0.04	53176.92	4.2 \pm 0.4	EIS
2004 June	53183.29	< 126	53182.27	51 \pm 3	53182.75	< 0.04	-	-	EIS
2004 July	53187.23	< 117	53187.30	15 \pm 2	-	-	-	-	-

Table 2. The VLA 4.9 GHz radio detections and a selection of upper limits (3σ) together with the corresponding quasi-simultaneous observations in optical (R band) and X-ray (PCA/RXTE and HEXTE/RXTE) bands.

Date	MJD radio [day]	Flux density radio [μ Jy]	MJD optical [day]	Flux density optical [μ Jy]	MJD PCA [day]	Flux PCA [10^{-9} erg cm $^{-2}$ s $^{-1}$]	MJD HEXTE [day]	Count rate HEXTE [c s $^{-1}$]	X-ray state
1990 August	48111.23	289 \pm 24	-	-	-	-	-	-	-
2002 March	52355.67	154 \pm 17	52354.87	302 \pm 10	52355.84	1.40 \pm 0.20	52356.69	2.3 \pm 0.4	IS
2002 April	52379.58	< 105	-	-	-	-	-	-	-
2002 May	52399.54	< 93	52400.82	16 \pm 2	-	-	-	-	-
2004 May	53151.42	< 255	53151.35	793 \pm 24	53151.71	1.97 \pm 0.13	53151.71	17.1 \pm 0.4	EIS
2004 June	53162.37	< 276	53162.38	540 \pm 17	53162.67	2.41 \pm 0.20	53162.67	17.3 \pm 0.4	EIS
2004 June	53170.35	< 246	53169.40	440 \pm 14	53170.40	3.89 \pm 0.51	53172.37	0.6 \pm 0.5	BS
2004 June	53176.35	< 174	53177.15	121 \pm 5	53176.92	0.40 \pm 0.04	53176.92	4.2 \pm 0.4	EIS
2004 June	53183.29	< 282	53182.27	51 \pm 3	53182.75	< 0.04	-	-	EIS
2005 March	53446.71	< 159	-	-	-	-	-	-	-
2005 April	53465.54	245 \pm 29	53465.34	444 \pm 14	53465.66	1.13 \pm 0.11	53465.66	10.4 \pm 0.4	EIS
2005 April	53472.50	317 \pm 30	-	-	53472.81	2.70 \pm 0.47	53472.81	19.5 \pm 0.4	EIS
2005 May	53494.52	< 156	53492.33	228 \pm 8	53493.79	0.84 \pm 0.07	53493.79	6.7 \pm 0.3	EIS
2005 May	53506.48	< 207	53508.31	107 \pm 5	53505.85	0.09 \pm 0.01	-	-	EIS

energy bands: A: 2.0–3.5 keV; B: 3.5–6.0 keV; C: 6.0–9.7 keV; D: 9.7–16.0 keV. The colours and intensity were defined as: soft colour $SC=B/A$, hard colour $HC=D/C$, intensity $I=A+B+C+D$. We applied dead-time corrections and subtracted the background using *pcabackest* (version 3.6), the latest models and updated SAA history files¹. Following the recommended procedure², we used the faint source model when the source was below ~ 40 c/s/PCU and the bright source model otherwise.

The PCA gains changed several times during the lifetime of RXTE, generating different “gain epochs”. On top of

these sudden changes, a long term gain decay is also present (Jahoda et al. 2006). In order to confidently compare count rates measured at different epochs, months to years apart, we normalized the count rates to those of the Crab nebula, which is known to be a steady X-ray source. The conversion from count rate to Crab was done using the value of the Crab rate closest in time and within the same PCA gain epoch (e.g. Kuulkers et al. 1994; van Straaten et al. 2003). To obtain the unabsorbed flux in the 2–10 keV band we extracted background and dead-time corrected PCA spectra using only PCU 2, as it has been the most active and best calibrated throughout the RXTE mission. We estimated the background spectra and created response matrices using *pcabackest* (as explained above) and *pcarsp*, respectively (both part of the same HEASOFT v. 6.5 package), and

¹ http://heasarc.gsfc.nasa.gov/docs/xte/pca_news.html

² http://heasarc.gsfc.nasa.gov/docs/xte/pca_news.html#quick_table

added a 1% systematic error to all channels and grouped them in order to have a minimum of 20 counts per energy bin. We then fitted the spectra within XSPEC 11.3.2ag using the following model: $wabs*(bbody+diskbb+powerlaw)$, and fixing the hydrogen column density to $0.5 \times 10^{22} \text{ cm}^{-2}$ (Church & Balucińska-Church 2001). In one case the system was in quiescence and we determined the corresponding upper limit on the flux using an absorbed power-law to fit the unmodeled background (diffuse emission).

In addition, we extracted 20–200 keV dead-time and background corrected count rates from the HEXTE standard mode data, and averaged them within each observation. We averaged both rocking directions in order to measure the background spectrum during each observation. For the analysis in section 6 we used cluster B data (excluding detector 2, which was damaged in March 1996), while for the rest of the paper cluster A data (all detectors). This choice was determined by the periods of anomalous rocking of cluster A, which otherwise might have affected the long-term analysis done in section 6. The overall gain and response matrix of the HEXTE detectors are independent of time and hence no Crab nebula normalization was applied to the HEXTE data.

2.3 Optical

For the current work we used part of the data from the long-term monitoring campaign on Aql X-1 reported in Maitra & Bailyn (2008). Details of the data reduction and analysis can be found in section 2.1 of the aforementioned reference.

The R-band observations were taken using the ANDICAM³ instrument on the 1.0 m and 1.3 m Small and Moderate Aperture Research Telescope System (SMARTS) at Cerro Tololo Inter-American Observatory (CTIO). The data reduction was done via the standard IRAF pipeline developed for ANDICAM.

Around 83 percent of the quiescent R-band flux is estimated to come from the contaminating star (Welsh et al. 2000) and was thus subtracted from the total observed flux from all the observations.

For magnitude to flux conversion it was assumed that $R=0$ magnitude corresponds to 3064 Jy (Campins, Rieke & Lebofsky 1985; Bessell, Castelli & Plez 1998). In Chevalier et al. (1999) the colour excess of Aql X-1 was estimated as $E(B-V)=0.5 \pm 0.1$. The R-band extinction A_R was determined using the standard total to selective extinction coefficient $A_V/E(B-V)=3.1$ and the interstellar extinction law $A_R/A_V=0.748$ (Rieke & Lebofsky 1985; Cardelli et al. 1989).

3 MULTI-WAVELENGTH LIGHT CURVES

For the three radio detections in 1990 August no multi-wavelength information was available and therefore we do not discuss these data here. We only note that during the quasi-simultaneous detections at 4.9 and 8.4 GHz on MJD

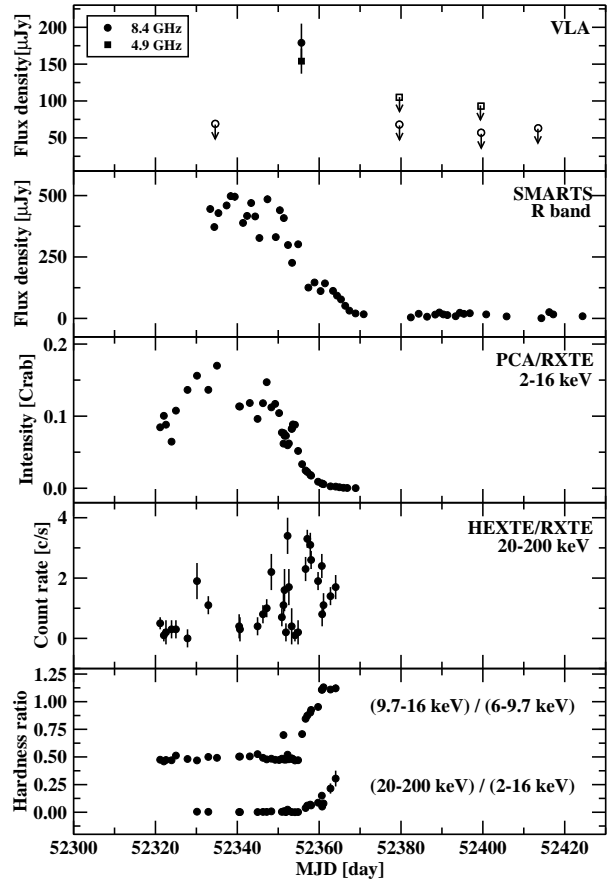


Figure 1. Multi-wavelength light curves for the outburst of Aql X-1 from 2002 March and the variation of the hardness ratio between two PCA bands (9.7–16 keV and 6–9.7 keV), and the HEXTE (20–200 keV) and PCA (2–16 keV) bands. If not appearing in the plots, the errors are smaller than the size of the points. The open symbols in the radio light curve denote 3σ upper limits.

48111.23 the spectrum through these frequencies was inverted (i.e. $\alpha \geq 0$ where $F_\nu \propto \nu^\alpha$).

3.1 2002 March outburst

During this outburst (Fig. 1) Aql X-1 was detected in radio quasi-simultaneously at 4.9 and 8.4 GHz and showed then an inverted spectrum. The optical and PCA data clearly indicate that the source was passing through an active state. It is also apparent that the beginning of the outburst was missed. The level of the HEXTE count rate is low during the ~ 40 days of monitoring and tends to rise slightly towards the end of the data set. As indicated by the hardness ratio, most of the period the system was in a soft state which it left suddenly and transited quickly to a hard state around

³ <http://www.astro.yale.edu/smarts/ANDICAM>

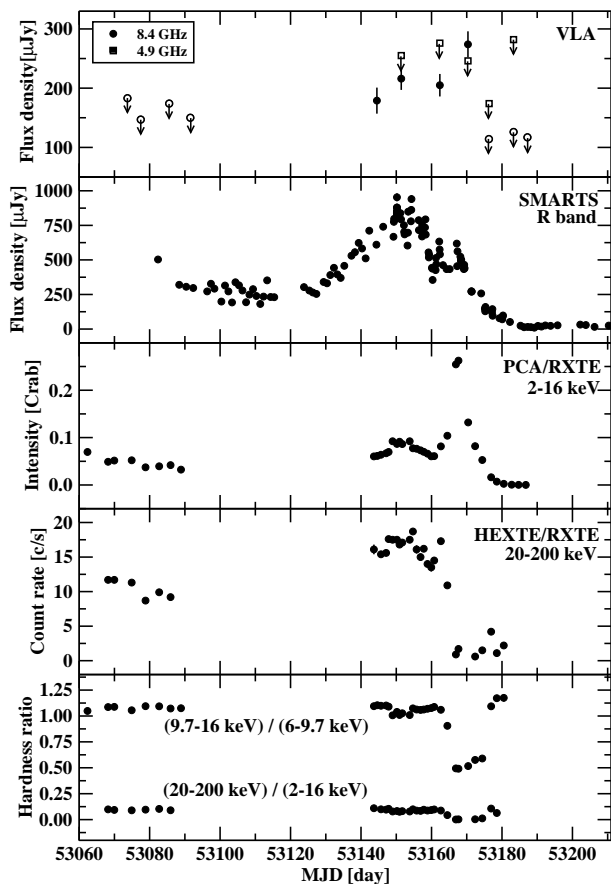


Figure 2. Multi-wavelength light curves for the outburst of Aql X-1 from 2004 May–June and the variation of the hardness ratio between two PCA bands (9.7–16 keV and 6–9.7 keV), and the HEXTE (20–200 keV) and PCA (2–16 keV) bands. If not appearing in the plots, the errors are smaller than the size of the points. The open symbols in the radio light curve denote 3σ upper limits.

MJD 52355. The radio detections are coincident with this X-ray state transition.

3.2 2004 May–June outburst

This is so far, relatively speaking, the most well covered outburst of Aql X-1 in the radio band (Fig. 2). The source was detected on 4 occasions and only at 8.4 GHz, however the lack of detection at 4.9 GHz might be partly attributable to the high rms noise due to the short integration times. On the epoch with the highest 8.6 GHz flux density detected, the quasi-simultaneous upper limit at 4.9 GHz allows us to constrain the spectrum in this frequency range to an inverted one. The optical light curve is well sampled and the PCA data reveal a major outburst preceded by a smaller flaring event at about MJD 53150. After an apparent peak, the HEXTE registered a drop in the count rate soon after the onset of the intensity increase in the PCA band. This has been observed before in Aql X-1 during two previous outbursts, by Yu et al. (2003). The hardness ratio diagram indicates that during the active period the system made a

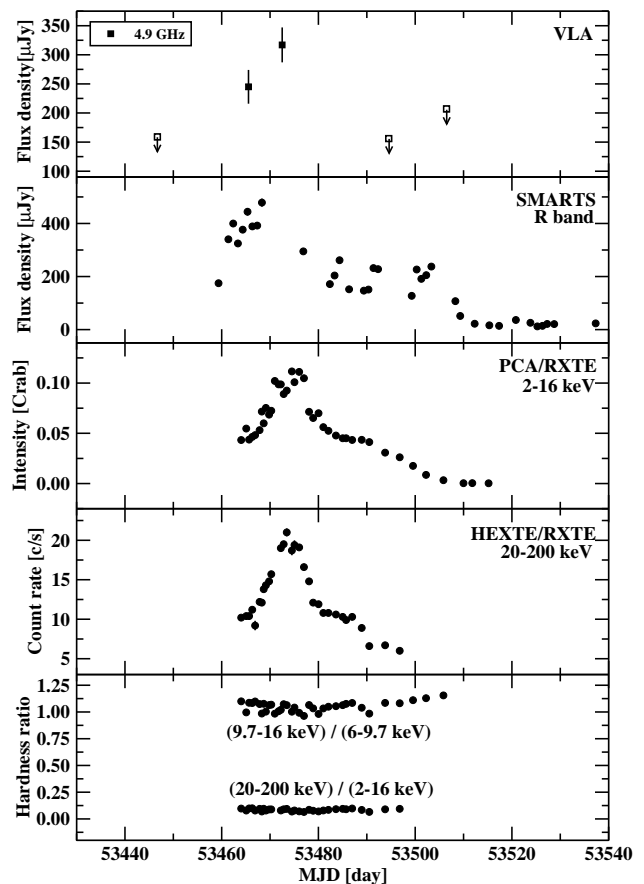


Figure 3. Multi-wavelength light curves for the outburst of Aql X-1 from 2005 April and the variation of the hardness ratio between two PCA bands (9.7–16 keV and 6–9.7 keV), and the HEXTE (20–200 keV) and PCA (2–16 keV) bands. If not appearing in the plots, the errors are smaller than the size of the points. The open symbols in the radio light curve denote 3σ upper limits.

series of X-ray state transitions, from hard to soft and back to hard. A similar behaviour is observed for the smaller flare, when the hardness ratio decreased by 10 percent, with the difference that in this case the system never reached the soft state, but only temporarily softened its spectrum. The increases in the radio flux density seem to trace the intensity enhancements in the PCA band.

3.3 2005 April outburst

For this outburst (Fig. 3), observations at 8.4 GHz were not available. Aql X-1 was detected twice at 4.9 GHz. The optical data is quite sparse and the onset of the burst was not covered well. The PCA and HEXTE intensity peaks are more or less coincident. The hardness ratio diagram reveals that the system never left the hard X-ray state during the active period.

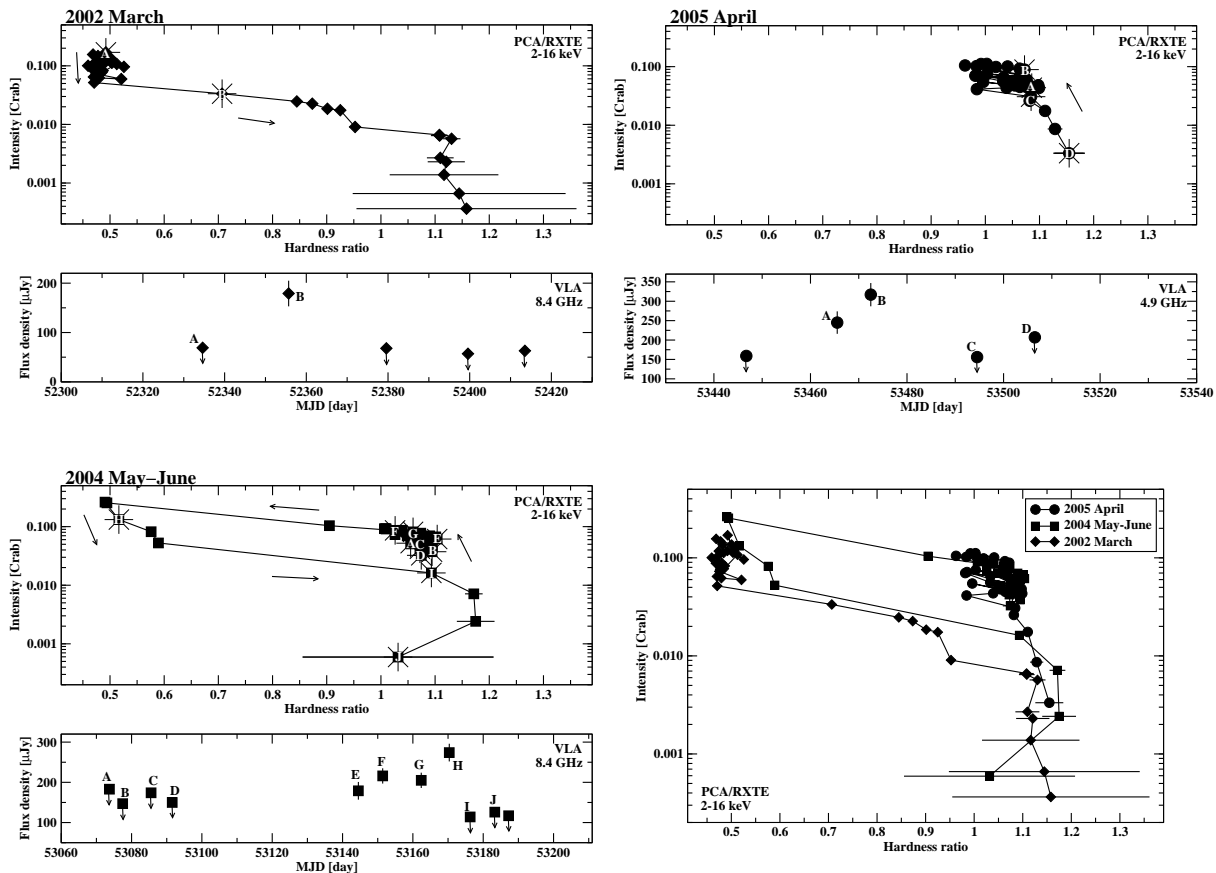


Figure 4. HIDs for the outbursts of Aql X-1 from 2002 March (upper-left; X-ray data between MJD 52321.1–MJD 52366.9), 2004 May–June (bottom-left; X-ray data between MJD 53053.8–MJD 53182.8) and 2005 April (upper-right; X-ray data between MJD 53464.0–MJD 53505.8). The cumulative HID for the all three outbursts is represented in the bottom-right panel. The hardness is the ratio of the count rates in the PCA bands 9.7–16.0 keV and 6.0–9.7 keV. The points highlighted in each HID are shown in the corresponding radio light curve. The other points do not correspond to quasi-simultaneous radio and X-ray observations.

4 HARDNESS–INTENSITY DIAGRAMS

The hardness-intensity diagrams (HIDs) corresponding to the three outbursts are represented in Fig. 4. The hardness ratio is the hard colour defined in section 2.2. Note that the scales for all the HIDs are identical. The system is tracing the HIDs counter-clockwise.

In 2002 March (Fig. 4, upper-left) the radio upper limit denoted “A” corresponds to a soft X-ray state of the system at a relatively high X-ray intensity. This situation is reminiscent of the similar behaviour observed in BHXRBS, when the radio emission is “quenched” above some X-ray flux level. We postpone a further discussion of the issue to section 6. The system stays in a soft X-ray state for a while and then makes a fast transition to a hard state. The radio detection (“B”) caught the system during this transitional phase.

In 2004 May–June (Fig. 4, bottom-left) the system traced a full cycle in the diagram. It looks similar to the HIDs observed in BHXRBS (e.g. Fender et al. 2004) and re-

cently in a dwarf nova (Körding et al. 2008). The first four radio non-detections (“A” to “D”) as well as the first three detections (“E” to “G”) correspond to a hard X-ray state. Then suddenly the system jumped to a soft X-ray state and the radio flux density increased significantly (“H”), by more than 30 percent (with the errors on the individual measurements of less than 10 percent). On a timescale comparable to the rise of the radio flux density, the system dropped below the radio detection limit, in a hard X-ray state (“I”, “J”).

In 2005 April (Fig. 4, upper-right) the system stayed constantly in a hard X-ray state. It experienced what is sometimes called a hard outburst (e.g. Migliari & Fender 2006). This has been observed in Aql X-1 on a few occasions (e.g. Rodriguez et al. 2006).

Fig. 4 clearly illustrates hysteresis in Aql X-1 (the X-ray luminosity at the transition from hard to soft state is different, i.e. higher, than the luminosity at the transition from soft to hard state). This kind of behaviour was previously noted for Aql X-1 (Maccarone & Coppi 2003; Maitra & Bailyn 2004; Gladstone, Done & Gierliński 2007). A HID with all the PCA data for all the X-ray outbursts of Aql X-1 between 1997 and 2008 clearly shows this (Fig. 5).

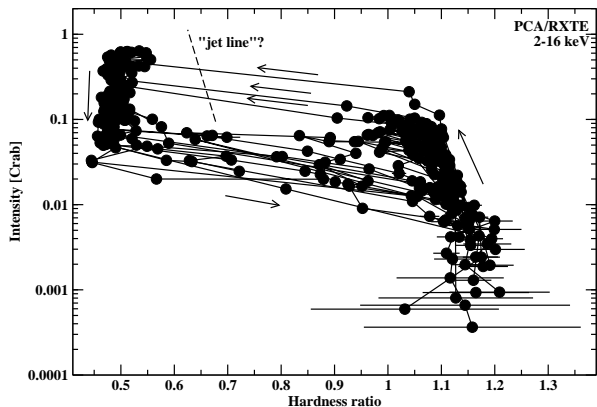


Figure 5. The cumulative HID for all the outbursts of Aql X-1 observed with the PCA/RXTE between 1997–2008. A hysteresis phenomenon is clearly at work in Aql X-1. The hardness is the ratio of the count rates in the PCA bands 9.7–16.0 keV and 6.0–9.7 keV. Superimposed (see section 7 for details) is the “jet line” of e.g. Fender et al. (2004).

Three major flares have been relatively well sampled and the corresponding hard to soft transitions in Fig. 5 are therefore not observationally biased. This phenomenon of hysteresis has been seen in BHXRBs (e.g. Rodriguez et al. 2003; Rossi et al. 2004; Belloni et al. 2005; Dunn et al. 2008) suggesting a common origin for the state transitions in NSXRBs and BHXRBs. In Fig. 5 the hard to soft transitions might appear to be significantly quicker than the soft to hard ones. This is an artifact due to the adding of the data together as some minor outbursts also follow tracks in the region between 0.01–0.10 Crab. Whether or not they trace a scaled down version of the large-scale diagram is not clear, but the superposition creates a region with a higher density of points, which could falsely be interpreted as symptoms of slower soft to hard transitions.

5 COLOUR–COLOUR DIAGRAMS

The colour-colour diagrams (CCDs) for the three outburst studied here in detail are shown in Fig. 6. The system is tracing the CCDs clockwise.

Already in Fig. 6 the CCD for the three outbursts hints that Aql X-1 seems to spend most of the time in two main X-ray states during the active periods: a harder state roughly with $HC > 0.9$, and a softer state with $HC < 0.6$ and a narrower interval of variation of SC. This is clearly confirmed by the CCD for all the outbursts observed with the PCA between 1997–2008 (Fig. 7). Besides the two main X-ray states, a transitional one is now evident, linking the two. This CCD is, not surprisingly, entirely consistent with the CCD built by Reig et al. (2004) with all the PCA data between 1997–2002 (note that we averaged the data over each observation). Following these authors and the nomenclature for atoll sources, we have identified the harder X-ray state

as the EIS, the softer one as the BS and the transitional state in between as the IS.

An almost complete cycle in the CCD was traced during the outburst in 2004 May–June (Fig. 6, bottom-left). Before the flare the system was in the EIS. As the count rate in the HEXTE band started to decline, the PCA intensity went up triggering a fast jump of the system to the BS. Aql X-1 stayed in this X-ray state for about 10 days and then, again relatively suddenly, within a couple of days, returned to the EIS via the IS. This kind of behaviour seems to be typical for many of the outbursts of Aql X-1 (see also Reig et al. 2004 who analyze in some detail different outbursts than we do here). Although some outbursts do not undergo a full cycle in the CCD, like the one on 2005 April (Fig. 6, upper-right), they do follow the same general trend in the CCD. The general pattern is the following: right before the onset of a major outburst in the PCA band the system is in the left side of the EIS, migrates towards the right side of the EIS and as the PCA intensity increases considerably it jumps suddenly to the BS. Here, moving towards its leftmost side (sometimes with excursions back to the right side), the peak of the PCA intensity is reached. Then, as the PCA intensity decreases the system jumps back to the EIS, passing quickly through the IS.

6 CORRELATIONS

Although established only for a limited sample of objects, a correlation seems to exist, extending over many orders of magnitude, between the X-ray and radio emissions of BHXRBs in the low-hard X-ray state (Corbel et al. 2003, 2008; Gallo et al. 2003, 2006). Recent evidence (Xue & Cui 2007; Gallo 2007) suggests that this correlation is not universal. More observations are definitely needed in order to settle the issue since given the relatively sparse nature of the data (particularly in the radio band) a confident conclusion cannot be reached at the moment. In the case of NSXRBs the situation is no better due to the fact that most of them systematically show weaker radio emission than BHXRBs (e.g. Fender & Kuulkers 2001). However, a correlation between the radio and X-ray emission has also been found for some of these objects in certain X-ray states, in particular the atoll source 4U 1728-34 (Migliari et al. 2003; Migliari & Fender 2006).

For Aql X-1 we have found indications in the data that also for this object a correlation seems to exist between the radio and X-ray bands. Given the small number of observations under consideration this should be taken as tentative only, subject to confirmation or refutation when more data will be available (particularly in the radio band). Fig. 8 shows the radio flux density versus the PCA X-ray flux for Aql X-1 (data from Tables 1 and 2). When the system was in the EIS, the 8.4 GHz data (3 points only) reveal that the radio and X-ray bands have a positive correlation with a correlation coefficient of 0.78. The slope of the correlation function is $\alpha = 0.29 \pm 0.23$ ($F_{radio} \propto F_X^\alpha$). Here and further on, the errors on the correlation function are standard errors of the regression fit. When considering only the 4.9 GHz data in the EIS (2 points only) the slope becomes 0.30. Taking

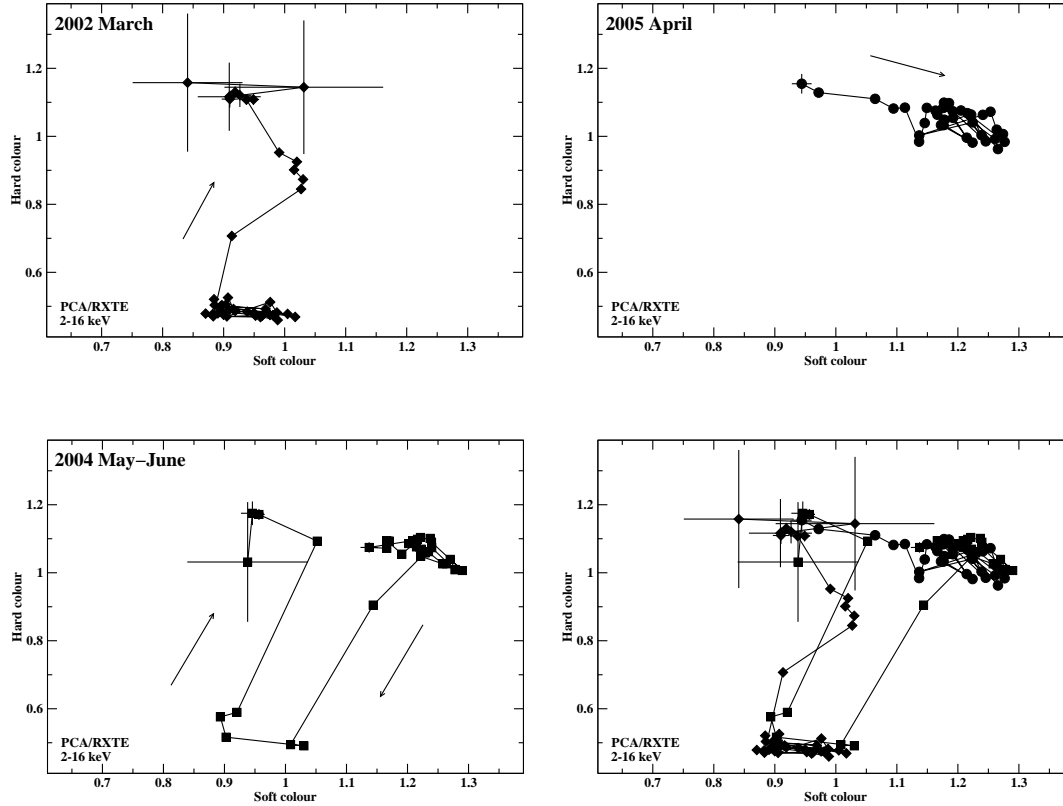


Figure 6. CCDs for the outbursts of Aql X-1 from 2002 March (upper-left; X-ray data between MJD 52321.1–MJD 52366.9), 2004 May–June (bottom-left; X-ray data between MJD 53053.8–MJD 53182.8) and 2005 April (upper-right; X-ray data between MJD 53464.0–MJD 53505.8). The cumulative CCD for the all three outbursts is represented in the bottom-right. The soft colour is the ratio between the count rates in the 3.5–6.0 keV and 2.0–3.5 keV bands and the hard colour is the ratio between the count rates in the 9.7–16.0 keV and 6.0–9.7 keV bands.

into account all the radio detections in the EIS, independent of the frequency (i.e. 5 points), the data show no correlation between the radio and X-ray bands (correlation coefficient 0.38). One possible explanation for this, assuming the correlation at 8.4 GHz is real, is that the spectrum between 4.9 and 8.4 GHz was not flat during these observations. In BHXRBs for instance, in general in the low-hard state the radio spectrum is flat or optically thick (e.g. Fender 2001), however in a few occasions it was observed that the spectrum changes rapidly and tends to become optically thin prior to a radio flare (Fender et al. 2004). Perhaps something similar happens in Aql X-1. Unfortunately, in our data set the only constraints to the radio spectrum comes from the observations of the outbursts from 2002 March (Fig. 1) and 2004 May–June (Fig. 3), when the system was not in the EIS. When all the 8.4 GHz data are taken into account, independent of the X-ray states of the system (i.e. 5 points), the slope of the correlation function is $\alpha=0.40 \pm 0.07$ with a correlation coefficient of 0.96 (dashed line in Fig. 8). A similar analysis, for all the 4.9 GHz data (3 points) reveals an at best marginal correlation (correlation coefficient 0.60) with a slope $\alpha=0.48 \pm 0.64$.

The radio upper limit denoted “Q1” in Fig. 8 is notable. It has a relatively high PCA flux and represents a deep radio upper limit. The system was in the BS at the time (point “A” in Fig. 4, top left). It looks as if the radio emission was “quenched”. A very similar situation is observed in some BHXRBs in the high-soft state, where the radio emission drops significantly above some X-ray flux (Gallo et al. 2003).

4U 1728-34 is the atoll source with the most numerous quasi-simultaneous detections in the radio and X-ray band (i.e. 10 up to now). We have used these data (VLA at 8.5 GHz with 100 MHz bandwidth, and PCA/RXTE in the energy band 2–10 keV) reported in Migliari et al. (2003) and Migliari & Fender (2006) to compare them against the Aql X-1 data from the point of view of the radio/X-ray correlations (Fig. 9). For Aql X-1, in calculating the luminosity we assumed the distance of 5.2 kpc used by Migliari & Fender (2006). A flat radio spectrum extending up to 8.5 GHz was also assumed. Following Migliari et al. (2003) and Migliari & Fender (2006), using all the data for 4U 1728-34 (except for the point denoted “Q2”) we found a positive correlation between the radio and X-ray bands, with the correlation coefficient 0.90 and the slope of the correlation function $\alpha=1.40 \pm 0.25$ ($L_{\text{radio}} \propto L_X^\alpha$), in perfect

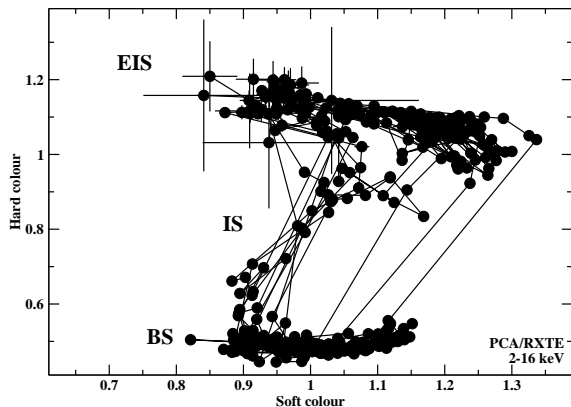


Figure 7. The cumulative CCD for all the outbursts of Aql X-1 observed with the PCA/RXTE between 1997–2008. While in the active state, the system spends most of the time in the “extreme island state” (EIS), with quick transitions through the “island state” (IS) and short excursions in the “banana state” (BS). The soft colour is the ratio between the count rates in the 3.5–6.0 keV and 2.0–3.5 keV bands and the hard colour is the ratio between the count rates in the 9.7–16.0 keV and 6.0–9.7 keV bands.

agreement with previous authors. If moreover we consider only the data corresponding to the hard state (i.e. 7 points; see Migliari & Fender 2006 for an identification of the X-ray states) the correlation coefficient becomes 0.96 and the slope 1.42 ± 0.20 . It seems therefore that the correlation function for Aql X-1 is flatter than the corresponding correlation function for 4U 1728-34. The normalization of the trends however, appears to be similar. This result seems to be significant, although given the very sparse data available at the moment in the radio band it is not possible to draw a solid conclusion. More radio observations are stringently needed in order to further constrain the correlation between the radio and X-ray bands for these sources.

As noted before by Migliari et al. (2003) the point “Q2” is interesting. It’s the highest PCA X-ray flux at which the radio counterpart was detected, and the radio emission is relatively weak. Moreover, the system was perhaps in a soft X-ray state, but this is not clear given the slightly contradictory spectral and timing properties (see the discussion in Migliari et al. 2003). Thus, it might be that the radio emission was “quenched” during this observation. The radio detection “Q2” of 4U 1728-34 and the radio upper limit “Q1” of Aql X-1 therefore suggest that NSXRBs might show a behaviour similar to BHXRBs with respect to the suppression of the radio emission above some X-ray flux levels.

No significant correlation was found between the radio and optical bands. The correlation coefficient for the 3 observations in 2004 May–June for which quasi-simultaneous data exists at radio (8.4 GHz) and optical wavelengths (see Table 1) in the EIS is 0.52. Adding also the observations in which the system was in the IS and the BS does not improve the correlation coefficient (0.01).

Maitra & Bailyn (2008) found correlations between the optical (R band) and ASM X-ray bands. The slope of the correlation function seems to be steeper when the system

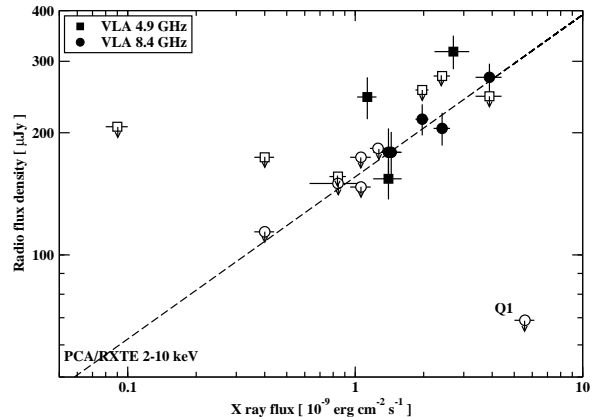


Figure 8. The radio/X-ray correlation in Aql X-1. The filled circles and squares correspond to the radio detections at 8.4 GHz and 4.9 GHz respectively. The empty symbols are the radio upper limits (3σ). The dashed line describes the correlation function (correlation coefficient 0.96) when taking into account all the 8.4 GHz detections independent of the X-ray state of the system, and has a slope $\alpha=0.40 \pm 0.07$ ($F_{radio} \propto F_X^\alpha$). The radio upper limit denoted “Q1” is discussed in section 6.

is in the hard state, however outliers are present and it’s not entirely clear what role, if any, the observational bias is playing. In turn, we were able to confirm this behaviour using PCA instead of ASM X-ray data (Fig. 10, top). All the multi-wavelength observations presented in Fig. 10 were quasi-simultaneous (separated by less than 1 day). The system in the EIS follows a different optical/X-ray correlation than in the BS.

Aql X-1 also shows distinct behaviours in the EIS and the BS X-ray states when the optical (R band) and HEXTE bands are compared (Fig. 10, middle). In the BS the HEXTE X-ray count rate is systematically low, independent of the optical flux. This is contrary to the trend observed in the PCA band where it is in the EIS that the system shows low X-ray intensities at very different optical flux levels (Fig. 10, top).

The interplay between the X-ray emission in the PCA and HEXTE bands can be seen in Fig. 10, bottom. Please note that in relation to Fig. 10 the term “correlation” was used loosely, more like in the sense of “trend”. Formally speaking, due to the scatter in the data, the correlation coefficients associated to Fig. 10 are not significant, with two exceptions: 0.93 for the optical/PCA X-ray bands in the BS (Fig. 10, top) and 0.95 for the HEXTE/PCA X-ray bands in the EIS (Fig. 10, bottom). Since only data during outbursts are available, and we only plotted the quasi-simultaneous observations (thus only part of the total amount of data was selected), the analysis might be biased, in particular in the top and middle panels of Fig. 10. More quasi-simultaneous multi-wavelength observations are needed in order to constrain the behaviour of Aql X-1.

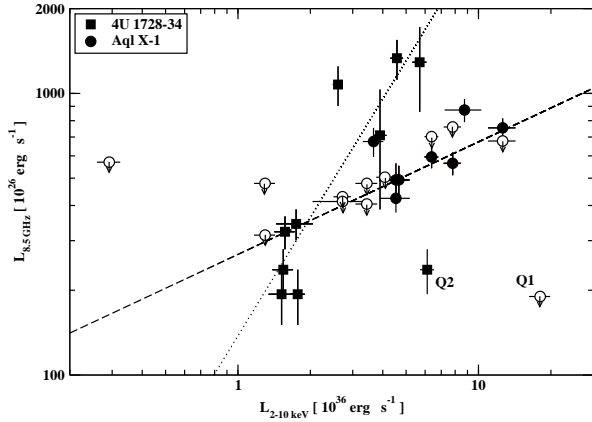


Figure 9. The radio (8.5 GHz)/X-ray (2–10 keV) correlations in Aql X-1 and 4U 1728-34. The filled circles and squares correspond to the radio detections of Aql X-1 and 4U 1728-34 respectively. The empty circles are the radio upper limits (3σ) for Aql X-1. The dotted line is the correlation function (correlation coefficient 0.90) for 4U 1728-34 (independent of the X-ray state) and has a slope $\alpha=1.40 \pm 0.25$ ($L_{radio} \propto L_X^\alpha$). The dashed line describes the correlation function (correlation coefficient 0.96) for Aql X-1 when taking into account all the 8.4 GHz detections independent of the X-ray state of the system and has a slope $\alpha=0.40 \pm 0.07$. The data points denoted “Q1” and “Q2” are discussed in section 6.

7 DISCUSSION AND CONCLUSIONS

Given the scarcity of the radio observations of Aql X-1 in the literature, we have searched the public VLA archive in the period 1986–2005 and found previously unreported detections thus bringing up the number of secure detections (more than 3σ) from 5 (Hjellming et al. 1990; Rupen et al. 2004, 2005) to 11. To attempt a multi-wavelength characterization of the system we used archival RXTE X-ray data (PCA and HEXTE) between 1997–2008 and the optical observations (R band) between 1998–2007 reported in Maitra & Bailyn (2008).

In the combined data set on Aql X-1 we found 3 outbursts for which quasi-simultaneous radio, optical and X-ray data exist (Figs. 1, 2 and 3). These light curves look quite different from each other, at all the wavelengths, showing that the source is revealing a rich phenomenology. Judging by the hardness ratio, the three outbursts under discussion can be considered as corresponding to distinct classes of outbursts: in 2002 March the radio flare can be associated to a soft to hard transition; in 2004 May–June to a “classical” hard to soft transition; and in 2005 April to a “hard flare”. In the optical band Maitra & Bailyn (2008) pointed out that the light curves of most of the outbursts of Aql X-1 do not belong to the pure fast rise exponential decay (FRED) topology and showed that FREDs occupy a particular region in the optical/X-ray plane that is distinct from the non-FRED outbursts.

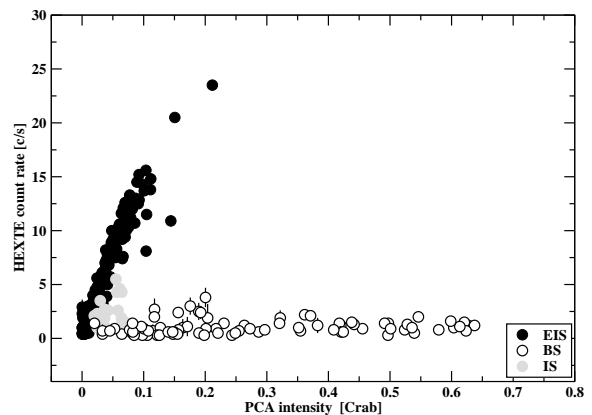
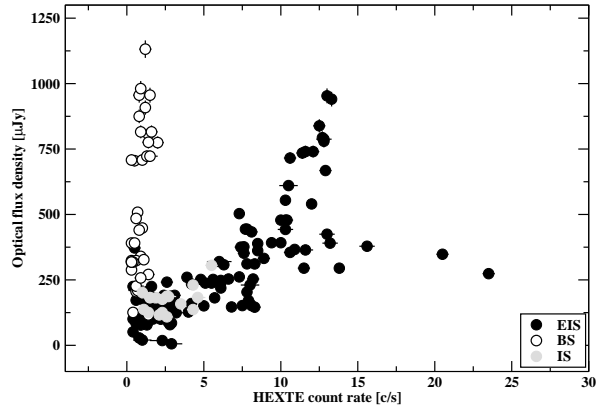
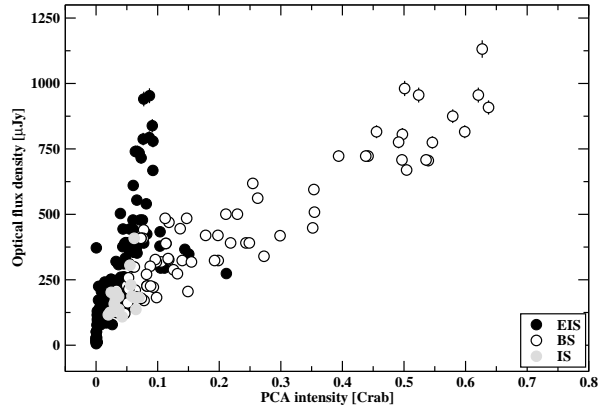


Figure 10. Trends in the behaviour of Aql X-1 in different X-ray states. Filled black circles correspond to the “extreme island state” (EIS), open circles to the “banana state” (BS) and filled gray circles to the “island state” (IS). All the observations in different bands are quasi-simultaneous (separated by less than 1 day). The used energy bands are 2–16 keV for the PCA/RXTE and 20–200 keV for the HEXTE/RXTE. The optical band is the R band.

But in spite of the diverse morphologies of the light curves, the outbursts of Aql X-1 tend to converge to a common behaviour when the HIDs and CCDs are investigated. The three outbursts presented in detail here, as well as most of the other events, track generally a similar path: counter-clockwise in the HIDs and clockwise in the CCDs. There might be nonetheless exceptions. In one case during a minor outburst in the soft state the system tracked partially the HID (Fig. 5, the left side of the diagram) clockwise. During two or three minor outbursts the system was transiting between the hard and soft states and back again within a very small range in the X-ray intensity (Fig. 5, the bottom side of the diagram, between 0.01–0.10 Crab) and it’s hard to say with certainty whether it mimicked a scaled down version of the diagram or was doing something completely different. The fact remains that the HIDs of Aql X-1 exhibit similar characteristics to the HIDs of some BHXRBS (e.g. Rodriguez et al. 2003; Rossi et al. 2004; Belloni et al. 2005; Dunn et al. 2008; Fender et al. 2009). For these objects a phenomenological model was developed that accounts for the connection between the radio and X-ray emission via the presence or absence of jets in the system (Fender et al. 2004, 2009). It goes as follows, starting from the lower right corner of the HID in Fig. 5. In the hard X-ray state a steady, optically thick jet is produced. During a typical outburst the X-ray intensity increases (moving up in the HID) and after a while the X-ray spectrum begins to soften (moving to the left in the HID). At the “jet line” the system enters the soft X-ray state when no jet is produced. The switching off of the jet is associated with relativistic ejections of matter, generally optically thin. The X-ray intensity decreases (moving down in the HID) and soon the X-ray spectrum starts to harden (moving right in the HID). At the crossing of the “jet line” the system switches on the steady jet and finishes the cycle back in the lower right corner of the HID. This kind of behaviour is roughly consistent with what is observed during the three outbursts of Aql X-1 (Fig. 4), but given the small number of radio detections it is practically impossible to test the model in more depth. The radio detection in a soft X-ray state with a likely inverted spectrum during the outburst from 2004 May–June (point “H” in Fig. 4, bottom left) does not necessarily contradict the idea of a turned off jet in the soft X-ray state since ad-hoc explanations are readily available, for instance by invoking a blob of matter ejected during the hard to soft transition at the “jet line”, which is expanding adiabatically (van der Laan 1966).

The presence of hysteresis in Aql X-1 has already been established (e.g. Maccarone & Coppi 2003; Maitra & Bailyn 2004; Gladstone et al. 2007) and confirmed in the present work (Fig. 5). Another atoll source, 4U 1608-522, shows a behaviour resembling that of Aql X-1 (Linares & van der Klis, in preparation). The similarity with the hysteresis phenomenon observed in BHXRBS (e.g. Rodriguez et al. 2003; Rossi et al. 2004; Belloni et al. 2005; Dunn et al. 2008) seems to suggest a common mechanism. What might be its nature is still a matter of debate. This is connected to the fact that at the moment, no self-consistent physical model of the X-ray states exists, although a few promising candidates are available (e.g. Remillard & McClintock 2006; Done, Gierliński & Kubota 2007 for reviews). Therefore the trigger of the transitions between these states, which is likely the mechanism responsible for the hysteresis, is still

an open issue (e.g. Done & Gierliński 2003; Zdziarski et al. 2004; Meyer-Hofmeister, Liu & Meyer 2005).

Evidence for radio/X-ray correlations were found in Aql X-1 (Fig. 8). Taking into account the radio detections at 8.4 GHz, the slope of the correlation function is $\alpha=0.40 \pm 0.07$ ($F_{radio} \propto F_X^\alpha$) with a correlation coefficient of 0.96. This is significantly different than the radio/X-ray correlation for another atoll source, 4U 1728-34 (Migliari et al. 2003; Migliari & Fender 2006), for which the data indicate a slope of 1.40 ± 0.25 with the correlation coefficient 0.90, although the normalizations of the correlation functions are similar for both sources. However, these results are based on a very limited sample of data points, 5 in the case of Aql X-1 and 9 for 4U 1728-34, and therefore need further testing with future observations. Nevertheless, it’s interesting to note that the slope of the correlations between the radio (8.5 GHz) and X-ray bands (2–10 keV) observed in some BHXRBS in the hard state are relatively close to what we obtained for Aql X-1: 0.51 ± 0.06 for V404 Cyg (Corbel et al. 2008), 0.58 ± 0.16 for A0620-00 (Gallo et al. 2006). But the normalizations of the correlation functions are higher for BHXRBS. This is related to the fact that the ratio between the radio and X-ray luminosity for BHXRBS is between one and two orders of magnitude higher than the corresponding ratio for NSXRBS (Fender & Kuulkers 2001; Migliari & Fender 2006). This can be explained for instance by a more efficient (i.e. “radio loud”) jet production mechanism in BHXRBS than in NSXRBS (Fender et al. 2003) which might come about due to the fact that the geometrically thick disks are more efficient at producing outflows (e.g. Meier, Koide & Uchida 2001) and the disks of NSXRBS are truncated at larger radii than those of BHXRBS. Or it might be that in the case of BHXRBS a large fraction of the extracted gravitational energy is advected across the event horizon, the end product of the process being more “X-ray quiet” systems (e.g. Narayan et al. 1997). From a more general point of view, it was shown that a scaling relation between the X-ray (2–10 keV) and radio (5 GHz) bands with a slope of 0.60 ± 0.11 holds for a fairly large sample of BHXRBS and active galactic nuclei (AGN) when the mass of the compact objects is taken into account (Merloni, Heinz & di Matteo 2003; Falcke, Körtling & Markoff 2004). Given also the recent advancements (e.g. the relation between the mass of the black hole, the accretion rate and the break frequency in X-ray power spectra for AGNs and XRBS [McHardy et al. 2006], or the similarity between the HIDs of XRBS and the HID of a dwarf nova in outburst [Körtling et al. 2008]), it seems that evidence is mounting at a fast pace that the accretion/ejection process works in a similar way in a broad class of objects: stellar mass black holes in XRBS, super-massive black holes in AGNs, and perhaps neutron stars in XRBS and white dwarfs in cataclysmic variables.

Aql X-1 shows evidence for the “quenching” of the radio emission in the soft X-ray state, above some X-ray flux (the radio upper limit “Q1” in Fig. 9). Migliari et al. (2003) found a similar behaviour in 4U 1728-34 (“Q2” in Fig. 9). Although it’s premature to jump to conclusions with such a limited sample, these are at least good indications that NSXRBS could mimic the behaviour of some BHXRBS from this point of view.

Maitra & Bailyn (2008) found a correlated behaviour between the optical (R band) and X-ray bands depending on

the state of the system. Using the same optical data set, and PCA X-ray data instead of ASM, we confirmed their findings. Moreover, we showed that trends exist also between the optical (R band) and HEXTE X-rays bands, and between the PCA and HEXTE bands (Fig. 10). Maitra & Bailyn (2008) proved that during the outbursts the evolution of the optical/infrared colour magnitude diagrams of Aql X-1 is consistent with thermal heating of an irradiated outer accretion disc. They noted that the optical/infrared colour and flux do not seem to change suddenly during the X-ray state transitions. This can be interpreted as evidence against a non-thermal origin of the optical/infrared emission. We didn't find any significant correlation between the optical (R band) and radio emission (at cm wavelengths), and although based on a very limited number of radio observations, this adds further support to this interpretation.

As a general remark, our data are roughly consistent with a truncated disc model of the X-ray states (e.g. McClintock & Remillard 2006 for a review). In hard X-ray states a standard accretion disc is truncated relatively far from the compact object. In soft X-ray states the disc is advancing closer to the innermost stable circular orbit. In the soft states the radiation is well described by black-body thermal emission from the inner regions of the accretion disc. But in the hard states the nature of the emitting material filling the gap between the compact object and the truncated disc (generically called the “corona”) is still under debate (e.g. Esin et al. 2001; Markoff et al. 2001; Blandford & Begelman 2004), although it is quite clear that synchrotron and Compton mechanisms are important. The fact that the optical emission (R band) does not seem to change significantly in the two X-ray states is further circumstantial evidence for the interpretation of Maitra & Bailyn (2008) of its origin as irradiation of the outer accretion disc.

ACKNOWLEDGMENTS

We thank the anonymous referee for detailed comments that improved the manuscript. The National Radio Astronomy Observatory is a facility of the National Science Foundation operated under cooperative agreement by Associated Universities, Inc.. This research has made use of data obtained through the High Energy Astrophysics Science Archive Research Center Online Service, provided by the NASA Goddard Space Flight Center.

REFERENCES

- Barret D., Boutelier M., Miller M.C., 2008, *MNRAS*, 384, 1519
- Belloni T., Homan J., Casella P., van der Klis M., Nespoli E., Lewin W.H.G., Miller J.M., Méndez M., 2005, *A&A*, 440, 207
- Berger M., van der Klis M., 1998, *A&A*, 340, 143
- Bessell M.S., Castelli F., Plez B., 1998, *A&A*, 333, 231
- Blandford R.D., Begelman M.C., 2004, *MNRAS*, 349, 68
- Campins H., Rieke G.H., Lebofsky M.J., 1985, *AJ*, 90, 896
- Cardelli J.A., Clayton G.C., Mathis J.S., 1989, *ApJ*, 345, 245
- Casella P., Altamirano D., Patruno A., Wijnands R., van der Klis M., 2008, *ApJ*, 674, L41
- Chevalier C., Ilovaisky S.A., 1991, *A&A*, 251, L11
- Chevalier C., Ilovaisky S.A., 1998, *IAU Circ.*, 6806, 2
- Chevalier C., Ilovaisky S.A., Leisy P., Patat F., 1999, *A&A*, 347, L51
- Church M.J., Balucińska-Church M., 2001, *A&A*, 369, 915
- Corbel S., Nowak M.A., Fender R.P., Tzioumis A.K., Markoff S., 2003, *A&A*, 400, 1007
- Corbel S., Körding E., Kaaret P., 2008, *MNRAS*, 389, 1697
- Cui W., Barret D., Zhang S.N., Chen W., Boirin L., Swank J., 1998, *ApJ*, 502, L49
- Czerny M., Czerny B., Grindlay J.E., 1987, *ApJ*, 312, 122
- Diamond P.J., 1995, in *ASP Conf. Ser. 82, Very Long Baseline Interferometry and the VLBA*, eds. J.A. Zensus, P.J. Diamond and P.J. Napier, p. 227
- Dickey J.M., Lockman F.J., 1990, *ARA&A*, 28, 215
- Done C., Gierliński M., 2003, *MNRAS*, 342, 1041
- Done C., Gierliński M., Kubota A., 2007, *A&ARev*, 15, 1
- Dunn R.J.H., Fender R.P., Körding E.G., Cabanac C., Belloni T., 2008, *MNRAS*, 387, 545
- Esin A.A., McClintock J.E., Drake J.J., Garcia M.R., Haswell C.A., Hynes R.I., Munro M.P., 2001, *ApJ*, 555, 483
- Falcke H., Körding E., Markoff S., 2004, *A&A*, 414, 895
- Fender R.P., 2001, *MNRAS*, 322, 31
- Fender R.P., Kuulkers E., 2001, *MNRAS*, 324, 923
- Fender R.P., Gallo E., Jonker P.G., 2003, *MNRAS*, 343, L99
- Fender R.P., Belloni T.M., Gallo E., 2004, *MNRAS*, 355, 1105
- Fender R.P., 2006, in *Cambridge Astrophysics Series, No. 39, Compact Stellar X-ray Sources*, eds. W. Lewin & M. van der Klis, p. 381
- Fender R.P., Homan J., Belloni T.M., 2009, *MNRAS*, 396, 1370
- Gallo E., Fender R.P., Pooley G.G., 2003, *MNRAS*, 344, 60
- Gallo E., Fender R.P., Miller-Jones J.C.A., Merloni A., Jonker P.G., Heinz S., Maccarone T.J., van der Klis M., 2006, *MNRAS*, 370, 1351
- Gallo E., 2007, in *The Multicoloured Landscape of Compact Objects and their Explosive Origins*, AIP Conf. Proc., vol. 924, p. 715
- Garcia M.R., Callanan P.J., McCarthy J., Eriksen K., Hjellming R.M., 1999, *ApJ*, 518, 422
- Gladstone J., Done C., Gierliński M., 2007, *MNRAS*, 378, 13
- Hasinger G., van der Klis M., 1989, *A&A*, 225, 79
- Hjellming R.M., Han X., Roussel-Dupre D., 1990, *IAU Circ.*, 5112, 1
- Hjellming R.M., Han X., 1995, in *X-ray Binaries*, eds. W.H. Lewin, J. van Paradijs, E.P.J. van den Heuvel, p. 308
- Högbom J., 1974, *ApJSS*, 15, 417
- Jahoda K., Markwardt C.B., Radeva Y., Rots A.H., Stark M.J., Swank J.H., Strohmayer T.E., Zhang W., 2006 *ApJS*, 163, 401
- Jonker P.G., Nelemans G., 2004, *MNRAS*, 354, 355
- Kitamoto S., Tsunemi H., Miyamoto S., Roussel-Dupre D., 1993, *ApJ*, 403, 315
- Körding E.G., Rupen M., Knigge C., Fender R., Dhawan V., Templeton M., Muxlow T., 2008, *Science*, 320, 1318

- Koyama K., Inoue H., Makishima K., Matsuoka M., Murakami T., Oda M., Osgawara Y., Ohashi T., Shibazaki N., Tanaka Y., Marshall F.J., Kondo I.S., Hayakawa S., Kunieda H., Makino F., Masai K., Nagase F., Tawara Y., Miyamoto S., Tsunemi H., Yamashita K., 1981, *ApJ*, 247, L27
- Kuulkers E., van der Klis M., Oosterbroek T., Asai K., Dotani T., van Paradijs J., Lewin W.H.G., 1994, *A&A*, 289, 795
- Maccarone T.J., Coppi P.S., 2003, *MNRAS*, 338, 189
- Maitra D., Bailyn C.D., 2004, *ApJ*, 608, 444
- Maitra D., Bailyn C.D., 2008, *ApJ*, 688, 537
- Markoff S., Falcke H., Fender R., 2001, *A&A*, 372, L25
- Martí J., Mirabel I.F., Rodriguez L.F., Chaty S., 1998, *A&A*, 332, L45
- McClintock J.E., Remillard R.A., 2006, in *Cambridge Astrophysics Series*, No. 39, *Compact Stellar X-ray Sources*, eds. W. Lewin & M. van der Klis, p. 157
- McHardy I.M., K rding E., Knigge C., Uttley P., Fender R.P., 2006, *Nature*, 444, 730
- Meier D.L., Koide S., Uchida Y., 2001, *Science*, 291, 84
- M ndez M., van der Klis M., Ford E.C., 2001, *ApJ*, 561, 1016
- Merloni A., Heinz S., di Matteo T., 2003, *MNRAS*, 345, 1057
- Meyer-Hofmeister E., Liu B.F., Meyer F., 2005, *A&A*, 432, 181
- Migliari S., Fender R.P., Rupen M., Jonker P.G., Klein-Wolt M., Hjellming R.M., van der Klis M., 2003, *MNRAS*, 342, L67
- Migliari S., Fender R.P., Rupen M., Wachter S., Jonker P.G., Homan J., van der Klis M., 2004, *MNRAS*, 351, 186
- Migliari S., Fender R.P., 2006, *MNRAS*, 366, 79
- Moore C.B., Rutledge R.E., Fox D.W., Guerriero R.A., Lewin W.H.G., Fender R., van Paradijs J., 2000, *ApJ*, 532, 1181
- Narayan R., Garcia M.R., McClintock J.E., 1997, *ApJ*, 478, L79
- Olive J.F., Barret D., Boirin L., Grindlay J.E., Swank J.H., Smale A.P., 1998, *A&A*, 333, 942
- Priedhorsky W.C., Terrell J., 1984, *ApJ*, 280, 661
- Prins S., van der Klis M., 1997, *A&A*, 319, 498
- Reig P., M ndez M., van der Klis M., Ford E.C., 2000, *ApJ*, 530, 916
- Reig P., van Straaten S., van der Klis M., 2004, *ApJ*, 602, 918
- Remillard R.A., McClintock J.E., 2006, *ARA&A*, 44, 49
- Rieke G.H., Lebofsky M.J., 1985, *ApJ*, 288, 618
- Rodriguez J., Corbel S., Tomsick J.A., 2003, *ApJ*, 595, 1032
- Rodriguez J., Shaw S.E., Corbel S., 2006, *A&A*, 451, 1045
- Rossi S., Homan J., Miller J.M., Belloni T., 2004, *Nucl.Phys.B*, 132, 416
- Rupen M.P., Mioduszewski A.J., Dhawan V., 2004, *ATel*, 286, 1
- Rupen M.P., Mioduszewski A.J., Dhawan V., 2005, *ATel*, 491, 1
- Rutledge R.E., Bildsten L., Brown E.F., Pavlov G.G., Zavlin V.E., 2001, *ApJ*, 559, 1054
- Shahbaz T., Casares J., Charles P.A., 1997, *A&A*, 326, L5
- Shahbaz T., Thorstensen J.R., Charles P.A., Sherman N.D., 1998, *MNRAS*, 296, 1004
- Shepherd M.C., 1997, in *ASP Conf. Ser.* 125, *Astronomical Data Analysis Software and Systems VI*, eds. G. Hunt and H.E. Payne, p. 77
- Šimon V., 2002, *A&A*, 381, 151
- van der Klis M., 1989, *ARA&A*, 27, 517
- van der Klis M., 1994, *ApJS*, 92, 511
- van der Laan H., 1966, *Nature*, 211, 1131
- van Straaten S., van der Klis M., M ndez M., 2003, *ApJ*, 596, 1155
- Welsh W.F., Robinson E.L., Young P., 2000, *AJ*, 120, 943
- Xue Y.Q., Cui W., 2007, *A&A*, 466, 1053
- Yu W., Li T.P., Zhang W., Zhang S.N., 1999, *ApJ*, 512, L35
- Yu W., Klein-Wolt M., Fender R., van der Klis M., 2003, *ApJ*, 589, L33
- Zdziarski A.A., Gierliński M., Mikołajewska J., Wardziński G., Smith D.M., Harmon B.A., Kitamoto S., 2004, *MNRAS*, 351, 791
- Zhang W., Jahoda K., Kelley R.L., Strohmayer T.E., Swank J.H., Zhang S.N., 1998, *ApJ*, 495, L9